Separation and Purification Technology 406 (2026) 139029

Contents lists available at ScienceDirect

Separation and Purification Technology

journal homepage: www.elsevier.com/locate/seppur

Ceramic ultrafiltration membrane with low palladium loading via atomic layer deposition for micropollutant degradation

Shuo Zhang [a,*], Ming Li [b], He Tian [a,c], J. Ruud van Ommen [b], Luuk C. Rietveld [a], Sebastiaan G.J. Heijman [a]

[a] Section of Sanitary Engineering, Department of Water Management, Faculty of Civil Engineering and Geosciences, Delft University of Technology, Stevinweg 1, 2628 CN Delft, the Netherlands
[b] Chemical Engineering Department, Faculty of Applied Sciences, Delft University of Technology, Van der Maasweg 9, 2628 HZ Delft, the Netherlands
[c] Chinese Academy of Environmental Planning, Ministry of Ecology and Environment, Beijing 100041, China

ARTICLE INFO

Editor: Junyong Zhu

Keywords:
Ceramic ultrafiltration
Peroxymonosulfate
Organic micropollutants
Atomic layer deposition
Low catalyst loading

ABSTRACT

Catalytic ceramic membranes are regarded as a promising technology for removal of organic micropollutants (OMPs). However, excessive catalyst loading will decrease membrane flux and increase deposition costs, thus hindering practical application. In this work, ceramic ultrafiltration membranes were modified by atomic layer deposition to achieve a low loading of palladium (Pd) for OMP degradation. The Pd deposited on the membrane surface and within the pores was used to activate peroxymonosulfate (PMS) to induce reactive species (RS) for the degradation of four OMPs (benzotriazole, diclofenac, sotalol, and trimethoprim). The Pd-deposited membranes exhibited an almost complete degradation of the four OMPs at a high flux of 100 L/(m^2 h). Notably, Pd confined within membrane nanopores induced a pronounced nano-confinement effect, enhancing degradation kinetics by up to three orders of magnitude compared to surface-deposited Pd, revealing a distinct catalytic mechanism governed by confined reaction environments. Varying RS can be generated from PMS activation by Pd-modified alumina membranes, but the dominant RS pathways were found to depend on the type of OMPs, providing new mechanistic insight into PMS activation in heterogeneous catalytic membrane systems. A high degradation efficacy was achieved at a pH of 7, while the PMS dosage (20–80 μM), anion (1 mM Cl^-, SO_4^{2-}, HCO_3^-, or ClO^-), and natural substances in river water had a minor impact on the OMPs' degradation. However, considerably high salinity, e.g., as present in brine water, exhibited a negative impact on the degradation of certain OMPs. This study demonstrates that a robust and effective strategy for OMPs' degradation can be achieved by ceramic membranes with a low loading of catalysts, which shows strong potential for cost-effective and scalable application in water treatment.

1. Introduction

Organic micropollutants (OMPs), present in drinking and source water, have a potentially adverse effect on human health and the environment. These OMPs, often originating from pharmaceuticals, personal care products, and industrial processes, can persist in water, and their removal by conventional wastewater treatment methods is challenging [1]. Membrane-based processes have been widely used in water treatment due to their compact design, and small footprint, among other advantages [2,3]. In contrast to nanofiltration and reverse osmosis membranes, ultrafiltration (UF) membranes operate at low pressures, resulting in reduced energy consumption and operational expenses. Additionally, UF membranes can maintain a high flux under low pressures, and their ability to be backwashed simplifies the cleaning and maintenance. However, UF membranes usually do not remove OMPs, because of their large pore sizes (10–100 nm). The rejection of benzotriazole (BT) by UF, from surface water, e.g., was only in the range of 29%–44% [4]. The low rejection of OMPs by UF membranes underscores the need for additional treatment strategies to effectively remove these OMPs.

To address the challenges of the low OMPs' removal, the integration of catalytic membranes with advanced oxidation processes (AOPs) has been explored to promote the degradation of OMPs. Unlike chlorine, which relies mainly on selective direct oxidation and often produces

* Corresponding author at: Department of Water Management, Building 23, Stevinweg 1, 2628 CN Delft, the Netherlands.
E-mail address: jszhangshuo@sina.com (S. Zhang).

https://doi.org/10.1016/j.seppur.2026.139029
Received 10 April 2026; Received in revised form 12 June 2026; Accepted 20 June 2026
Available online 24 June 2026

harmful by-products, AOPs utilize highly reactive species (RS) to non-selectively mineralize a broad range of OMPs with minimal toxic byproduct formation [5,6]. Among various AOPs, peroxymonosulfate (PMS) is a promising oxidant with a high redox potential (1.82 V), compared to 1.76 V for H_2O_2, thereby enabling more effective degradation of OMPs.

Although catalytic membranes coupled with AOPs have garnered attention, the excessive loading of catalysts on the membrane can result in substantial flux loss and the inhibition of OMPs degradation. For instance, ceramic UF membranes experienced a flux loss of 20% to 66% after being coated with a TiO_2 photocatalyst [7]. The high flux loss due to the thick catalytic coating was also found by Ma et al. [8]. In addition, Feng et al. have found that the highest degradation kinetics of 1,4-dioxane were found at the lowest Pd/Al_2O_3 loading (0.02 g/L) [9]. The negative effects, caused by the high loading of catalysts, have been attributed to the quenching effect of catalytic surfaces on the formed RS. A decrease in OMP degradation due to overloaded catalysts was also reported by Berger et al. [7]. Moreover, excessive catalyst loading will significantly increase the coating costs. To reduce the loading of catalysts, recent studies have explored the integration of single-atom catalysts to enhance the performance of catalytic membranes [8,10]. However, single-atom catalysts still suffer from limited stability, challenges in dispersion control, and difficulties in scalable fabrication, which hinder their large-scale application in catalytic membranes [11]. Therefore, it requires a practical and cost-effective strategy to modify the membrane with low catalyst loading, which is crucial to promote the application of catalytic membranes in water treatment.

Atomic layer deposition (ALD) is a precise thin-film deposition technique that allows for the controlled modification of membranes at the atomic level [7]. In addition, the conformal coating achieved by ALD can ensure uniform coverage of catalysts across the entire membrane structure, including the membrane surface and internal pores, thereby increasing the catalytic surface areas [12,13]. Currently, ALD has been employed to load catalysts onto membranes for the degradation of OMPs, but most studies report considerable flux loss due to high catalyst loadings [7,13]. Moreover, excessive catalyst loading may diminish catalytic efficacy and increase operational costs. To overcome these limitations, low catalyst loadings achieved via ALD have been explored in electrocatalytic applications, where they have demonstrated high efficacy [14–16]. Nevertheless, it remains unclear whether such low loadings can enhance the performance of catalytic membranes in PMS activation for OMPs' degradation. Among various metal catalysts, Pd/Al_2O_3 is an effective catalyst in PMS activation, which can achieve a higher degradation of OMPs compared to other catalysts [17]. In addition, Pd can be deposited at relatively low and controllable growth rates via ALD, enabling precise ultralow-loading catalyst deposition, which makes it a promising candidate for low-loading catalytic membranes. For example, the Pd growth rate via ALD (0.15–0.2 Å/cycle) is lower than that of TiO_2 photocatalysts (≈0.3 Å/cycle), which allows for more precise deposition and a lower catalyst loading [7,18]. This allows membranes to be modified with an ultra-low catalyst loading, which can reduce cost and minimize flux loss that typically caused by thick coating. In addition, excessive catalyst loading can inhibit OMP degradation. Therefore, low Pd loading via ALD will be an effective strategy for simultaneously enhancing catalytic activity and catalyst utilization efficiency. However, studies on Pd-deposited Al_2O_3 ceramic membranes, particularly those employing ultra-low Pd loadings, are still limited.

Moreover, in the PMS activation, different RS can be induced, such as $^{\bullet}OH$, $SO_4^{\bullet-}$, $^1O_2$, and $O_2^{\bullet-}$ [19]. However, in the Pd/Al_2O_3-PMS system, the currently identified dominant RS remains controversial. A non-radical pathway was identified for 4-chlorophenol, whereas the surface-bound sulfate radical was found to dominate in the degradation of 1,4-dioxane [9,20]. This may result from the focus on the degradation of individual OMP in previous studies, which likely led to these inconsistent conclusions regarding the dominant RS in the same system. Therefore, further investigation is needed to clarify the contribution of individual RS in the Pd/Al_2O_3-PMS system to the degradation of multiple OMPs.

Hence, this study aims to load a low amount of Pd on the surfaces and in the pores of ceramic UF membranes by ALD to activate PMS for the degradation of four selected OMPs, being benzotriazole (BT), diclofenac (DIC), sotalol (SOT), and trimethoprim (TMP). To assess the influence of Pd deposited in pores, kinetic experiments were performed with only flow over the membrane surface and experiments with flow over the membrane surface and through the pores. The most important RS were determined by quenching experiments, where different scavengers were used to quenching corresponding RS. In addition, parameters such as pH, PMS dosage, and ions, potentially affecting the performance, were studied. Finally, OMPs were spiked into brine and river water to evaluate the degradation performance in complex water matrices.

2. Materials and methods

2.1. Ceramic UF membranes

Single-channel tubular ceramic UF membranes (CoorsTek, the Netherlands), with a pore size of 20 nm (CoorsTek data), were used in this study. The membranes consist of top and support layers made of Al_2O_3, having an internal diameter of 7 mm, an outer diameter of 10 mm, and a length of 100 mm. To avoid membrane leaking during the filtration experiments, a two-component epoxy adhesive (Araldite AW 5047–1 and Hardener HW 5067–1, from VIBA, Netherlands) was used to seal the two edges of the membranes (10 mm for each side).

The Pd-deposited ceramic UF membranes (Pd-UF) were achieved via ALD in a custom-built, atmospheric-pressure flat-substrate ALD reactor [21–23]. The reactor chamber consists of a metal cylinder with an inner diameter of 40 mm and a length of 190 mm. To maintain a uniform temperature profile during deposition, temperature was monitored and controlled using two thermocouples placed inside and outside the reactor. Atmospheric-pressure ALD was selected over vacuum-based ALD to lower capital costs and improve scalability and throughput [22,23]. The Pd deposition procedure was adapted from previous work [18], with modifications to the reaction time and precursor gas flow rate based on our own requirements. The ALD precursors, $Pd(hfac)_2$ (Sigma-Aldrich) and formalin (Sigma-Aldrich), were contained in stainless steel bubblers. High-purity nitrogen (99.999%) was used as both the carrier and purging gas, flowing parallel to the substrate surface inside the reactor. $Pd(hfac)_2$, formalin, and ultrahigh purity nitrogen (99.999%) were used as the precursor, co-reactant, and purging gas, respectively. Before initiating Pd deposition, the ALD reactor was stabilized at 200 °C. The time sequence of the one-cycle ALD used in this study was 30–30–40–30 s. A gas mixture of 0.5 L/min of $Pd(hfac)_2$ and 0.5 L/min of N_2 was flowed over the membrane substrates for 30 s. 1 L/min N_2 was used to purge the excessive $Pd(hfac)_2$. After purging, 0.7 L/min formalin with 0.3 L/min N_2 was introduced for 40 s, followed by a purging step of 1 L/min N_2 for 30s, completing one cycle of ALD. The ceramic UF membranes deposited with Pd by 3, 30, and 60 cycles of ALD are denoted as C3, C30, and C60, respectively, while the pristine membrane is denoted as C0.

The pristine and modified membranes were characterized by scanning electron microscopy (SEM, Hitachi S-3400 II, Japan) with energy dispersive spectroscopy (EDS). X-ray photoelectron spectroscopy (XPS) was carried out to examine the inner surface of Pd-UF by using a Kα system (ThermoFisher Scientific) with a photon energy of 1486.7 eV. To eliminate the charging effect on peak shift, the carbon 1 s (C1s) spectrum peak at 284.8 eV was used as a reference to calibrate the XPS peak positions through CasaXPS software [24]. The porosity of the membrane and the thickness of the selective layer were estimated by the SEM image through the ImageJ analysis [25,26].

2.2. OMPs degradation experiments

2.2.1. Constant-flux setup

The filtration experiments were conducted using the setup shown in Fig. 1. The dead-end filtration system consisted of a feed tank (No. 1) containing a mixed solution of OMPs and PMS, a peristaltic pump (No. 2, Watson-Marlow, Netherlands) to deliver the feed, and a ceramic membrane module (No. 5). A needle valve (No. 3), installed in the recirculation line, was used to regulate the transmembrane pressure, which was monitored by a pressure gauge (No. 4), thereby controlling the permeate flux. A balance (No. 6, KERN, Germany) connected to a computer (No. 7) for data acquisition, enabling real-time determination of the permeate flux. To maintain a constant flux during filtration, the needle valve was adjusted throughout the experiment.

2.2.2. OMPs degradation during membrane filtration

Degradation of single OMPs over time. To have an insight into the removal of a single OMP over time, SOT (from Sigma-Aldrich) was selected as the model OMP. After adding 40 μM potassium PMS (from Sigma-Aldrich) solution into 5 μg/L SOT solution, the pH was adjusted with 0.1 M HCl and 0.1 M NaOH. This solution was used as a feed for the subsequent experiment. The filtration was first run for 5 min to achieve a stable fixed flux of 30 L/(m^2 h). Then the filtration experiment ran for 40 min. 5 mL permeate samples, taken at different time intervals to determine the SOT and PMS concentrations, were immediately injected with 50 μL 40 mM $Na_2S_2O_3$ (from Sigma-Aldrich) to terminate any oxidation.

Degradation of multiple OMPs by Pd-UF with PMS. The four OMPs were purchased from Sigma-Aldrich, and their properties are listed in Table 1 [1]. The selected OMPs (BT, DIC, SOT, and TMP) are pharmaceutical or pharmaceutical-related compounds commonly detected in surface water and wastewater [27]. However, traditional treatment cannot effectively remove these compounds [1]. As a result, they have been listed by the Dutch Ministry of Infrastructure and Water Management as target substances for evaluating the effectiveness of advanced treatment technologies for pharmaceutical removal from water [27]. Despite belonging to the same group, BT, DIC, SOT, and TMP exhibit different physicochemical properties such as molecular structures and charge characteristics at neutral pH, allowing evaluation of the Pd-UF-PMS system across representative pharmaceutical pollutants. The stock solution, containing the four OMPs, with a concentration of 1 mg/L for each, was diluted with demineralized water to 5 μg/L each. 5 mL of the prepared OMPs' solution was taken to determine the initial concentrations. Then the OMPs' solution mixed with 20, 40, or 80 μM PMS at pH of 2.5, 7, or 11, respectively, was filtered over Pd-UF for 5 min to achieve a stable fixed flux (i.e., 30, 100, 200, or 500 L/(m^2 h)). During the subsequent 40-min of filtration, 5 mL samples were taken from the permeate side and mixed with $Na_2S_2O_3$. Given that anions can affect AOP performance, the presence of 1 mM Cl^-, SO_4^{2-}, HCO_3^-, or ClO^- was also studied.

Effect of Pd deposited on the surface and in the pores. The role of Pd deposited on the membrane surface in OMPs' degradation was conducted by closing the permeate side and opening the concentration side (Fig. S1). As a result, the solution only flowed along the membrane surface from the feed side to the concentration side. In this case, OMPs were only degraded by the Pd deposited on the surface without the contribution of Pd deposited in the pores. The residence time was calculated by the tubular membrane length and the flow velocity from the feed side to the concentration side.

Scavenging experiments for RS identification. Based on earlier studies, different scavengers were dosed in the feed water to eliminate certain RS [30,31]. Tert-butanol (TBA), and methanol (MeOH) were used to quench RS of $^{\bullet}OH$, and both $^{\bullet}OH$ and $SO_4^{\bullet-}$, respectively, while furfuryl alcohol (FFA), and L-ascorbic acid (LAA) were used to scavenge $^1O_2$ and $O_2^{\bullet-}$, respectively. In the quenching experiment, scavenger was injected into the mixed OMPs and PMS solution, where the concentration of scavenger (0.4 mM) was 10 times higher than the concentration of PMS (40 μM).

Potential practical application. The applicability of the combined filtration-AOPs system was evaluated using real water types, including river water and two types of brines: brine A with low salinity and brine B with high salinity. The river water was collected from the canal Delftse Schie (Delft, the Netherlands) without pretreatment for the experiment, and brine A and B were simulated based on the earlier studies [32–34]. The total dissolved solids (TDS) were measured as 568 mg/L for river water, 4573 mg/L for brine A, and 22,867 mg/L for brine B. Detailed water quality parameters are provided in Table S1.

2.2.3. Water sample analysis

The UPLC-MS/MS system (Waters, ACQUITY UPLC I-Class, Xevo TQ-S micro fitted with the ESI) equipped with a C18 column (ACQUITY UPLC™ BEH 2.1 × 50 mm, 1.7 μm particle size) was employed to measure the concentration of the OMPs [1]. The PMS concentration was measured by adding 1.5 mL of a mixed solution containing 100 g/L KI and 5 g/L $NaHCO_3$ to 1.5 mL samples and was then tested by UV–Vis at 352 nm, as proposed by Liang et al. [35]. The calibrated curve of PMS concentration and corresponding UV spectra is shown in Fig. S2.

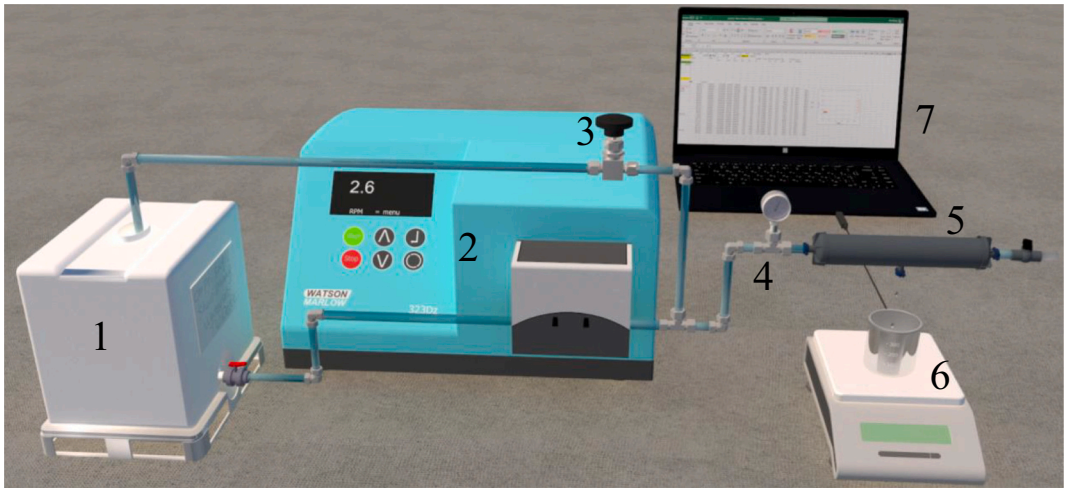

Fig. 1. Constant-flux setup for membrane filtration with components labeled as follows: (1) feed tank, (2) peristaltic pump, (3) needle valve, (4) pressure gauge, (5) membrane module, (6) balance, and (7) computer.

Table 1
Structure and properties of the selected OMPs [27–29].

Name	Molecular structure	Molecular weight (g/Mol)	$LogK_{ow}$	Charge (at pH 7)	Min./max. Projection radius (Å)
Benzotriazole (BT)		119	1.44	Neutral	3.66/4.12
Diclofenac (DIC)		296	4.51	Negative	4.62/6.34
Sotalol (SOT)	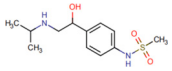	272	0.24	Positive	4.21/7.94
Trimethoprim (TMP)	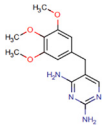	290	0.91	Positive	4.97/6.95

3. Results and discussion

3.1. Characterization of ceramic membranes

The top-view SEM image of the Pd-deposited membrane (C60) shows that, compared to the pristine membrane, hardly any morphological changes existed (Fig. 2a and b). This suggests that the Pd deposition process did not notably alter the membrane's surface structure, maintaining its original texture and integrity. The XPS (Fig. S12) and SEM-EDX (Fig. S13) analyses confirm the successful deposition of Pd on the inner pore structures of the C60 membrane.

Previous studies have demonstrated that Pd growth via ALD on Al_2O_3 exhibits highly reproducible and predictable cycle-dependent growth behavior. Such growth characteristics have been quantitatively investigated using highly sensitive techniques including quartz crystal microbalance, and rutherford backscattering spectroscopy [18,36,37]. Pd growth rates on Al_2O_3 are reported in the range of 0.15–0.2 Å/cycle with loading rates of approximately 1.841×10^{-5} mg/cm^2/cycle under comparable deposition conditions [18,36,37]. Therefore, the Pd loading in the present study was estimated based on these established ALD growth characteristics together with the applied ALD cycle number. This means that after 60 ALD cycles, the estimated Pd particle size was 0.9–1.2 nm, with a total Pd loading of 1.1×10^{-3} mg/cm^2. Given the ultralow Pd loading and the confinement of Pd within nanopores, direct quantitative determination of the absolute Pd loading remains experimentally challenging. Importantly, this study mainly focuses on

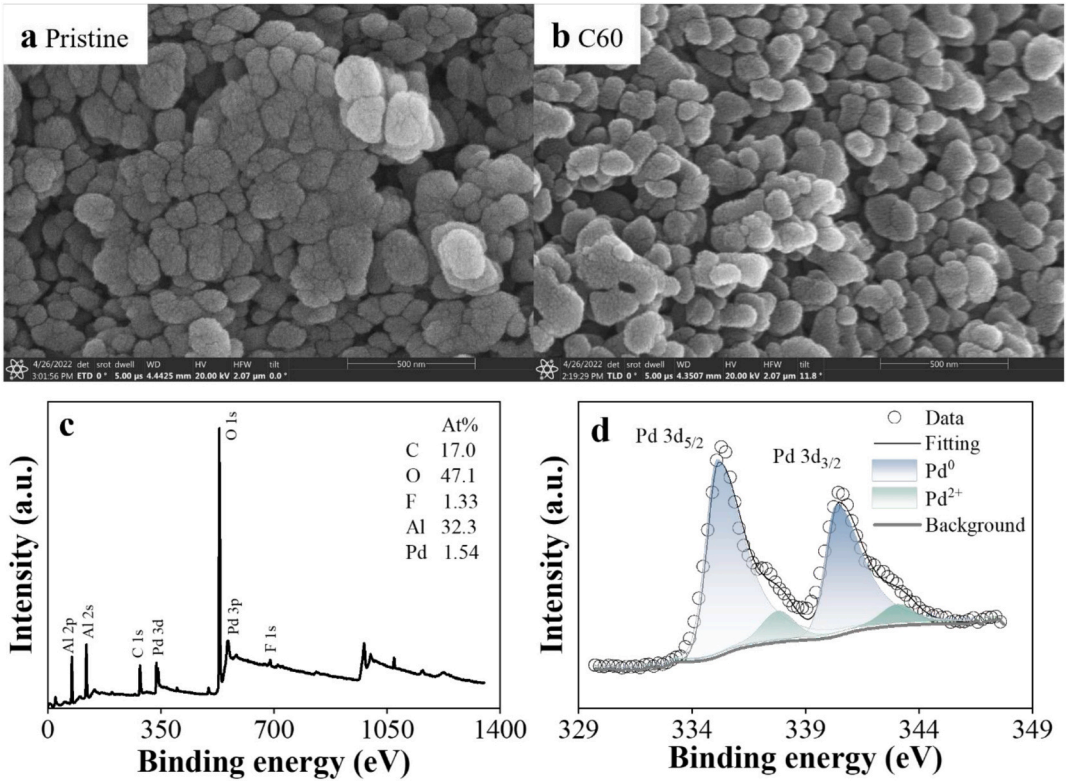

Fig. 2. SEM images of the membrane surface: (a) pristine and (b) C60 membranes; XPS spectra of C60: (c) full survey and (d) Pd 3d spectra.

exploring the performance of ceramic membranes with low catalyst loading enabled by ALD, rather than establishing a precise quantitative relationship between Pd loading and catalytic activity.

The full spectrum scan of XPS shows that Pd was successfully deposited on the membrane with Pd atomic ratios (ar.) of 1.36% (Pd/Al). The peak fit of the fine XPS spectra of Pd 3d was based on an earlier report, as shown in Fig. 2d [38]. The binding energy of 335.3 and 340.6 eV were ascribed to Pd^0, which accounted for 83.8% (ar. of Pd^0/ Pd), while 337.3 and 342.6 eV represented Pd^{2+} with an ar. of 16.2% (Pd^{2+}/ Pd) [39–41]. A 1.33% (ar.) of F was also found from the XPS full scan, which can be attributed to the formation of Al-O-Pd(hfac)* or HhFac during the ALD reaction process [18].

3.2. PMS activated by Pd-UF

Different membrane systems were first employed to evaluate their performance over filtration time for the degradation of contamination.

The pristine Al_2O_3 UF membrane (C0) and C60 Pd-UF were first examined at a flux of 30 L/(m^2 h). The degradation efficacy was calculated by Eq. S4. As shown in Fig. 3a, both C0 and C60 exhibited low rejections of SOT (5%–14%), attributed to the large pore size of the UF membrane (17.7–20 nm) compared to the size of SOT (< 1 nm). These findings align with the previous study, where it was reported that SOT rejection by UF membrane was in the range of 5%–32%, depending on the permeate flux [42]. In addition, the removal efficacy of SOT by the pristine membrane C0 with 40 μM PMS slightly increased to 20%, probably due to the direct oxidation by PMS [43]. The highest SOT removal efficacy, around 98%, was achieved by the C60 membrane with 40 μM PMS. This enhanced removal was likely due to the high oxidation potential of RS, such as $SO_4^{\bullet-}$, $^{\bullet}OH$, $^1O_2$, and $O_2^{\bullet-}$, induced by the catalyst-PMS system, with potentials ranging from 1.52 V to 3.1 V. To further evaluate the consumption of PMS in different systems, PMS concentration was measured during the filtration with the C0 and C60 membranes (Fig. 3b). The C0 membrane showed a gradual PMS decomposition from 27% at 3 min to 39% at 40 min, while the C60 membrane achieved a rapid PMS decomposition, ranging from 93% to 100% throughout the filtration process, also indicating the high efficacy of the C60 membrane in catalyzing PMS.

Fig. 3c shows the performance of the C3, C30, and C60 membranes in SOT degradation over time. All Pd-UF systems exhibited a rapid degradation of SOT. After 40 min, the C3 membrane achieved 52% SOT degradation, while the C30 and C60 membranes achieved comparable results, with 99% and 98% SOT degradation, respectively. The relatively low SOT degradation by the C3 membrane with PMS can be caused by the much lower loading of Pd to catalyze PMS into RS. Based on Lu and Stair, the loading of Pd on the C3, C30, and C60 membranes was 5.5×10^{-5}, 5.5×10^{-4}, and 1.1×10^{-3} mg/cm^2, respectively [36]. Once the membrane surface is uniformly covered with a certain loading of catalysts, additional deposition will not further increase the available reactive area. Consequently, it will not enhance PMS activation for OMP

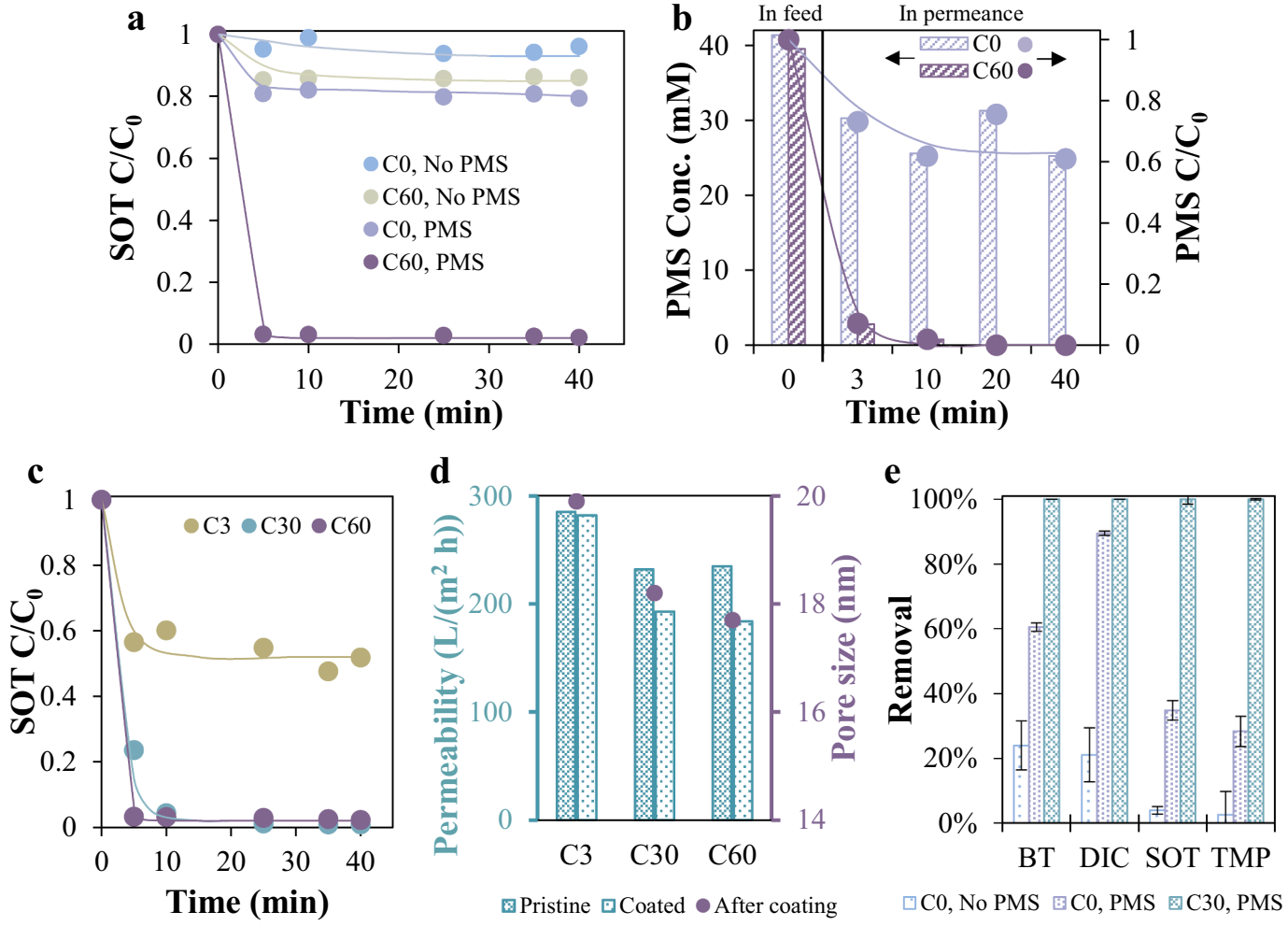

Fig. 3. Performance examination of different membrane systems in (a) SOT removal over time, and (b) PMS consumption by C0 or C60. (c) SOT removal over time by the membranes (C3, C30, and C60) modified by 3, 30, and 60 ALD cycles, respectively. (d) Pure water flux of pristine and deposited membranes. (e) Removal of four OMPs by different membrane systems. The experiments were conducted at the constant flux of 30 L/(m^2 h) with and without 40 μM PMS, at pH = 7.

degradation, as was evident after 30 ALD cycles. Feng et al. have reported that a high loading of Pd on the Al_2O_3 particles can even deteriorate the stoichiometric efficiency of PMS utilization due to the scavenging effect caused by the excess Pd [9].

Apart from the similar SOT degradation efficacies between the C30 and C60 membranes, the C30 membrane exhibited a smaller permeability decrease, from 232 to 193 L/(m^2 h bar), compared to the C60 membrane, from 235 to 184 L/(m^2 h bar) (Fig. 3d). This can be contributed to the low loading of Pd, which has a limited effect on the pore sizes (Fig. 3d). The representative pore sizes of the C30 and C60 membranes, for example, were estimated to be 18.2 nm and 17.7 nm, respectively, using the Carman-Kozeny equation (Eq. S1) developed for membranes [44]. It should be noted that the calculated pore sizes are just indicative values: they were estimated based on the assumption that the entire membrane structure was uniformly deposited by Pd, without altering membrane tortuosity or porosity due to the much lower loading. These calculated pore sizes were comparable to the values estimated based on the pore narrowing due to the deposited Pd particle size (Fig. S3). Given that the C30 membrane shows higher permeability and efficient degradation, and lower chemical use for coating, it was selected for further experiments.

The capacities of C0 and C30 with and without PMS in the removal of the four selected OMPs are shown in Fig. 3e. Without PMS, the C0 membrane removed 3%–24% of the four OMPs. With PMS, the removal of BT, SOT, and TMP by the C0 membrane increased to 61%, 35%, and 28%, respectively, while DIC removal reached 90%, likely because PMS

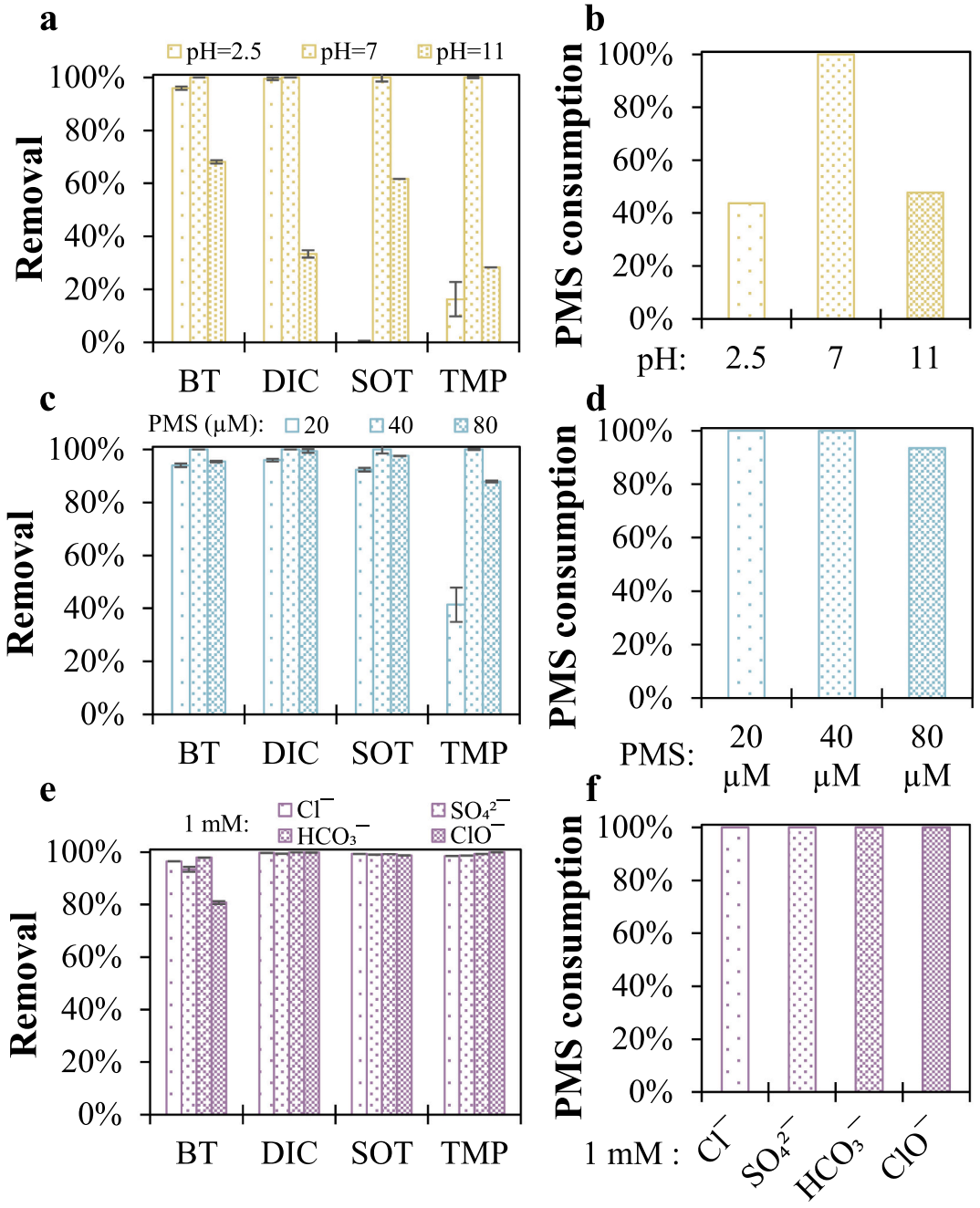

Fig. 4. OMP removal and PMS consumption under different conditions: (a) OMP removal at different pH values; (b) PMS consumption at different pH values; (c) OMP removal at different PMS concentrations; (d) PMS consumption at different PMS concentrations; (e) OMP removal in the presence of different anions (1 mM); and (f) PMS consumption in the presence of different anions (1 mM). Unless otherwise specified, experiments were conducted using the C30 membrane at a constant flux of 30 L/(m^2 h) with 40 μM PMS at pH 7 and an initial OMP concentration of 5 μg/L for each compound.

can directly oxidize DIC. From Fig. 3e, the removal of OMPs by the pristine C0 membrane without PMS can be attributed to adsorption, while the OMPs' removal by C0 with PMS can be caused by the direct oxidation by PMS [43,45]. It shows that adsorption likely accounted for 3%–24% OMPs' removal, while direct oxidation by PMS increased the removal efficacies of BT, SOT and TMP to 28%–44% and that of DIC to 89%. In contrast, when the C30 membrane was coupled with PMS, it achieved an almost complete removal of all OMPs.

To evaluate the operational stability of the membrane, a continuous filtration experiment was conducted for 10 h (Fig. S14a). The removal efficacies remained consistently high throughout the operation, with no noticeable decline observed. In addition, the leaching test (Fig. S14b) showed that Pd leaching was as low as 1.9 μg/L, which is significantly lower than the leaching level of Al (15.3 μg/L) from the pristine membrane, indicating strong immobilization of Pd on the ceramic membrane. These results confirm the membrane's excellent operational and structural stability.

3.3. Influence of pH, PMS concentration, and co-existing ions

The effects of pH, PMS concentration, and anion can play a role in the oxidation process [43]. Hence, variations of pH (2.5, 7, and 11), PMS concentrations (20, 40, and 80 μM), and ions (Cl^-, SO_4^{2-}, HCO_3^-, and ClO^-) were examined, respectively, for their impact on OMP degradation and PMS activation, as shown in Fig. 4 and Fig. S4.

Although the degradation efficacy of BT and DIC exhibited a small decrease at a pH of 2.5, the degradation efficacies of SOT and TMP reduced considerably at a pH of 2.5, while the degradation of all four OMPs was reduced at a pH of 11 comparing to the performance at a pH of 7 (Fig. 4a). Kang et al. have also found that in the α-Fe_2O_3-PMS system, the highest OMPs' degradation was achieved at a pH = 7, and the pH lower or higher than 7 has a negative influence on OMPs' degradation [46]. Dong et al. also reported that in the $MoSe_2$-PMS system, the most effective pH for PMS was in the range of 4 to 9, while the OMPs' oxidation is reduced prominently when pH < 3 or > 11 [47]. The oxidation of OMPs at a pH of 2.5 and 11 can be ascribed to the inhibited consumption of PMS, since PMS decomposition was reduced from 100% at a pH of 7 to 44% and 48% at a pH of 2.5 and 11, respectively (Figs. 4b and S4a). Compared to conventional Fenton processes that generally require acidic conditions, PMS-based AOPs show that this system can operate efficiently under neutral pH, avoiding pH adjustment. Besides, neutral pH conditions are representative of most natural waters [48] and practical water treatment scenarios [49], which suggests that the Pd-UF-PMS system shows promise for real-world applications.

The degradation of TMP decreased considerably to 41% and 88% at PMS concentrations of 20 and 80 μM, respectively, while the degradation of the three other OMPs remained relatively high, ranging from 92% to 100% across PMS concentrations of 20, 40, and 80 μM (Fig. 4c). Although PMS was completely depleted at 20 and 40 μM, its consumption decreased to 90% at 80 μM (Figs. 4d and S4b). This decline is likely due to the limited catalytic surface area, which was insufficient to activate the excess PMS at higher concentrations.

It has been reported that anions can inhibit the degradation of OMPs due to the reaction between anions and radicals [50]. However, when 1 mM anions of Cl^-, SO_4^{2-}, HCO_3^-, or ClO^- were present in the system, the degradation of most OMPs remained as high as 93%–100%, while only the degradation of BT was reduced to 81% in the presence of ClO^- (Fig. 4e). Figs. 4f and S4c show that none of these anions inhibited the PMS consumption. This can be attributed to the excess radicals formed in the membrane pores, which probably compensated for any potential interference caused by the anions [51].

3.4. Effective degradation of OMPs at high flux

The flux, related to the residence time, can impact the OMPs' degradation in the coupled the catalyst-PMS system [52]. Therefore, fluxes of 30, 100, 200, and 500 L/(m^2 h) were employed over the C30 membrane for 40-min filtration. The flux as a function of filtration time is shown in Fig. S10. The residence time was calculated by the permeate flux, porosity of the membrane (Fig. S5), and thickness of the selective layer (Fig. S5) with Eq. S2.

Below 100 L/(m^2 h), almost complete degradation of the four OMPs was achieved. As the flux increased to 500 L/(m^2 h), the degradation efficacies of BT and TMP decreased considerably (Fig. 5a), e.g., at fluxes of 200 and 500 L/(m^2 h), BT was only degraded by 81% and 51%, respectively. This was likely due to the reduced residence time of the PMS and OMPs across the membrane at a higher flux. As a result, it led to a decrease in the contact opportunities between PMS and the Pd catalyst, as well as between the formed RS and OMPs. The removal of BT, DIC, SOT, and TMP by different membranes at varying fluxes, as obtained from literature, is summarized in Fig. 5b and Table S2. The high removal of the four selected OMPs is typically achieved by membranes with small pore sizes, such as nanofiltration and reverse osmosis membranes, at a low flux (4–55 L/(m^2 h)). In contrast, UF membranes, due to their larger pore sizes, generally exhibited low rejection of these small-sized OMPs. When Pd-UF was coupled with PMS, its performance became comparable to that of nanofiltration and reverse osmosis membranes. Besides, the high removal of OMPs was achieved by Pd-UF at a much higher flux while operated at a low transmembrane pressure.

To further compare the proposed system with other studies, AOP-catalytic membrane systems reported in the literature were summarized in Table S4, including catalyst loading, flux, and removal efficiency. In general, high removal efficiencies are often achieved at relatively high catalyst loadings or lower flux. For example, most systems require loadings above 0.01 mg/cm^2, and in some cases up to hundreds of mg/cm^2, to maintain high degradation performance. In contrast, the Pd loading in this study (5.5×10^{-4} mg/cm^2) is several orders of magnitude lower than those reported catalytic membranes, and also significantly lower than previously reported ultra-low-loading catalysts (0.08–0.2 mg/cm^2). Considering that catalyst materials are the dominant cost component in catalytic membranes, this ultra-low loading directly translates to a substantially reduced material cost. Despite this ultra-low loading, our system achieves complete removal at a relatively high flux (100 L/(m^2 h)), outperforming most reported catalytic membrane systems for OMP removal (Table S4 and Fig. S11).

PMS consumption measured in the permeate side was maintained at 98%–100% during 40-min filtration through the C30 membrane at a flux of 30 L/(m^2 h) (Fig. 5c). This suggests that the Pd deposited by ALD on the membrane was stable for continuous catalysis of PMS. However, it was found that PMS consumption decreased with an increased flux. At fluxes of 30, 100, 200, and 500 L/(m^2 h), PMS decomposition was 99%, 87%, 74%, and 43%, respectively (Fig. 5c and d). The decline of PMS decomposition, and thus OMP degradation,at fluxes above 100 L/(m^2 h) can be attributed to the decreased retention time (Fig. 5d). Moreover, increasing the flux could dilute the RS retained within the pores, thereby reducing the degradation efficacy of OMP.

3.5. Important role of Pd deposited in the pores

It was expected that Pd deposited in the pores promotes the contact of reactants with the Pd catalyst and subsequently of the RS with the OMPs [51]. To gain insight into the contribution of Pd deposited on the membrane surface compared to the Pd in the pores, experiments were conducted to study this effect. The effect of Pd on the surface and within the pores was studied using the setup with and without permeate flow (Fig. 1 and S1), i.e., experiments involving flow exclusively over the membrane surface and flow both over the surface and through the pores.

When both the Pd on the surface and inside the pores were involved in the catalytic reactions (i.e., with permeate flow), almost 100% of the four OMPs were degraded within a retention time of 162 ms (at 100 L/(m^2 h)), as shown in Fig. 5a and d. However, when only Pd on the membrane surface was involved, the degradation efficacy of the four

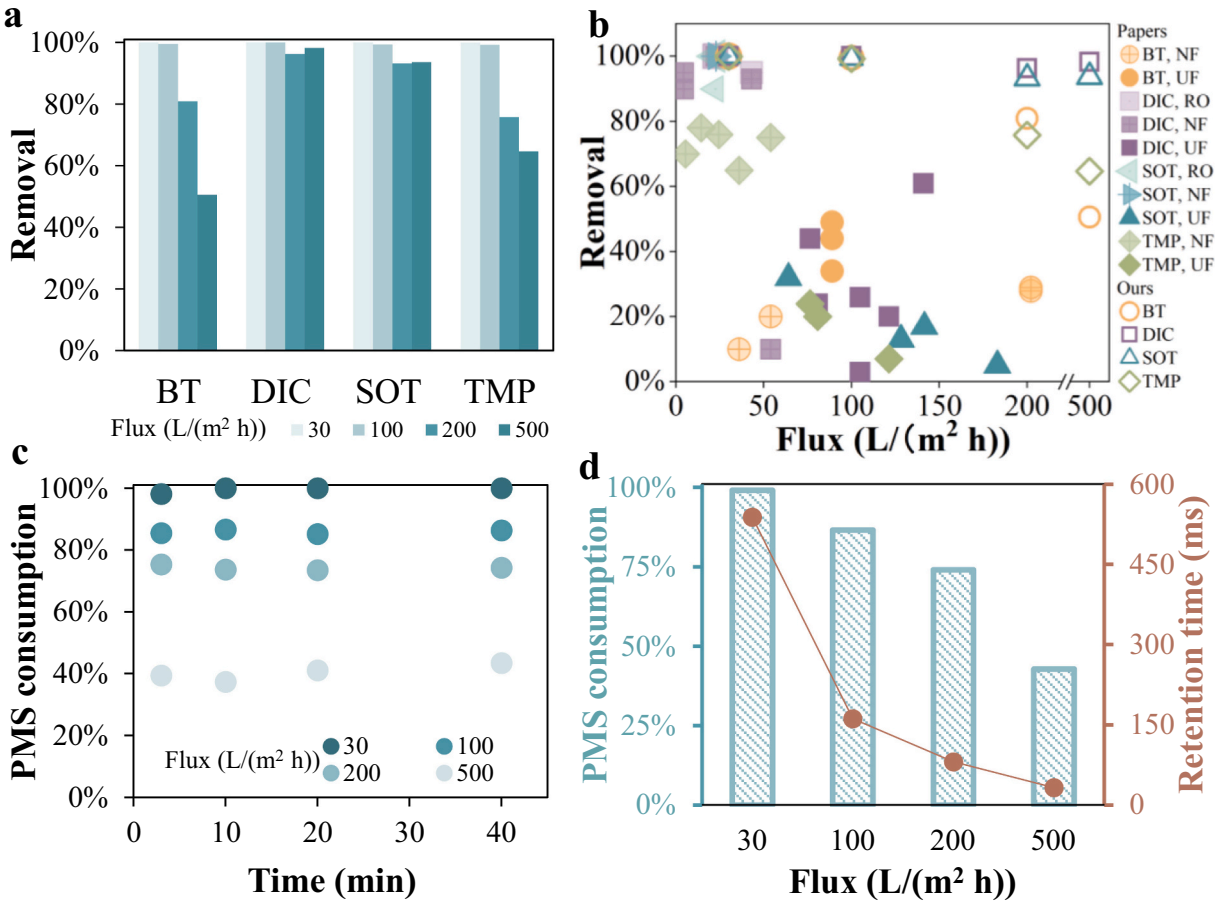

Fig. 5. Performance of the C30 membrane coupled with PMS at varying fluxes. Removal of four OMPs at different fluxes; (b) comparison of OMP removal performance between the membrane developed in this study and membranes reported in the literature (Table S2); (c) PMS consumption over time; and (d) PMS consumption and retention time at varying fluxes. The experiments were conducted using a mixed OMP solution containing 5 μg/L of each compound and 40 μM PMS at pH 7. The solution was filtered through the C30 membrane for 40 min under varying flux conditions, while the applied flux was maintained at the designated value throughout the experiment.

OMPs was less than 12%, even with an extended retention time (859–2412 ms) (Fig. 6a). This low removal can be attributed to the limited diffusion of RS from the active areas to the bulk, as reported by previous study [53].

The degradation kinetics of the four OMPs by the sole Pd on the membrane surface, and Pd on the surface and in the pores, are revealed in Fig. 6b and Fig. S6a and b, using Eq. S3 for the calculation. The kinetic constants of BT, DIC, SOT, and TMP were 4.2×10^{-5}, 3.6×10^{-5}, 6.0×10^{-2}, and 2.2×10^{-2} $(ms)^{-1}$, respectively, for Pd on the surface. However, the kinetic constants of OMPs degradation, achieved by Pd on the surfaces and in the pores, reached 0.028, 0.050, 0.034, and 0.030 $(ms)^{-1}$ for BT, DIC, SOT, and TMP, respectively. This suggests that the presence

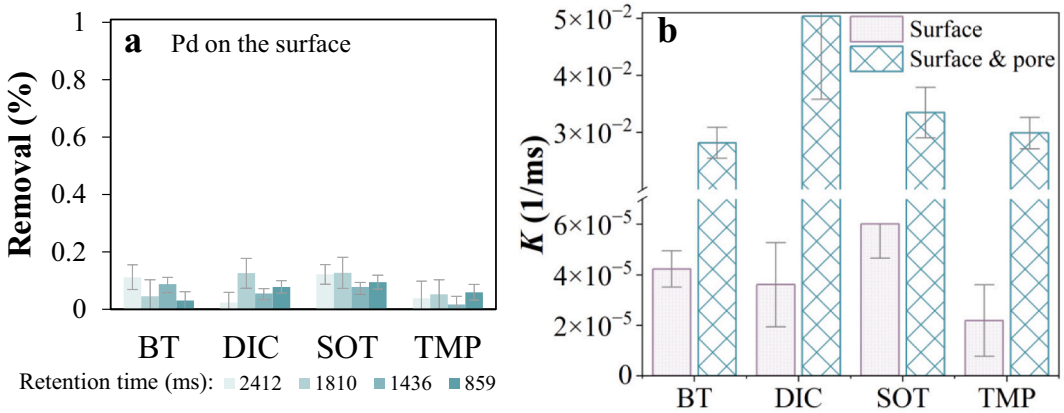

Fig. 6. (a) Removal of OMPs by Pd deposited on the membrane surface at different residence times. (b) Kinetic constant comparison of OMPs' degradation with and without the involvement of Pd deposited in the pores. The performance of Pd on the surface was evaluated by feeding OMPs (5 μg/L for each OMP) and 40 μM PMS over the C30 membrane surface by closing the permeate side.

of Pd within the pores enhanced the kinetics by three orders of magnitude. This kinetic enhancement is consistent with an earlier study, where Fenton degradation kinetics of para-chlorobenzoic acid was increased by a factor of 107 when Fe_3O_4 was also deposited in 20 nm pores [51]. The high kinetic degradation, facilitated by Pd in the pores, can be attributed to the nanoconfinement effect. Studies have shown that the concentration of RS is highly dependent on the distance from the catalytic regions, with RS concentration increasing when RS is confined in nanopores, thereby promoting their mass transfer [51,54]. The enrichment of RS induced by the nanoconfinement effect is further supported by the estimated RS concentration gradient derived from the reaction-diffusion model (Text S3), which indicates that nanoscale pores restrict RS diffusion distances and promote their accumulation within the pores. The membrane pores also provide abundant catalytic surface areas to trigger the formation of RS to degrade the nearby OMPs enriched within the pores.

3.6. Dependence of OMPs degradation on the types of RS

Scavengers are typically used to identify the dominant RS in PMS activation. However, there are varying conclusions regarding the dominant RS generated by alumina-supported Pd catalysts. Feng et al. have reported that $SO_4^{\bullet-}$ and $^{\bullet}OH$ were the primary RS responsible for the degradation of 1,4-dioxane [9], whereas Ahn et al. have found that both $SO_4^{\bullet-}$ and non-radical pathways played dominant roles in the degradation of 4-chlorophenol [17,20]. These studies, however, only focused on the degradation of individual OMP, which likely overlooks the synergistic effects of different RS in the degradation of multiple OMPs, especially in real water containing complex mixtures of OMPs. Therefore, to study the influence of the RS, $SO_4^{\bullet-}$, $^{\bullet}OH$, $^1O_2$, and $O_2^{\bullet-}$, on the degradation of multiple OMPs by the Pd/Al_2O_3-PMS system, TBA, MeOH, FFA, and LAA were used as their scavengers, respectively. Electron paramagnetic resonance (EPR) coupled with spin trapping is widely used technique for RS identification in heterogeneous catalytic systems. However, EPR was not performed in the present study. Recent reassessments of RS detection in catalytic membrane reactors have also shown that short residence times may limit complete reactions between RS and spin traps, while unstable adducts such as DMPO-OOH can decompose during transport from the membrane reactor to the EPR instrument [55]. In addition, the relatively low PMS concentration (40 μM) employed in this study likely resulted in low steady-state RS concentrations, which may complicate reliable EPR signal detection and interpretation, as EPR is typically designed to detect RS at μM level [56]. Previous studies on heterogeneous PMS activation systems have reported that steady-state RS concentrations were in the range of 10^{-8}–10^{-7} μM under 50–120 μM PMS [57,58]. Furthermore, although EPR can detect the formation of RS, it is difficult to directly determine which RS is mainly responsible for the degradation of individual OMP in complex systems containing multiple OMPs [55,56,59]. We therefore employed scavenger-based quenching experiments, a widely accepted

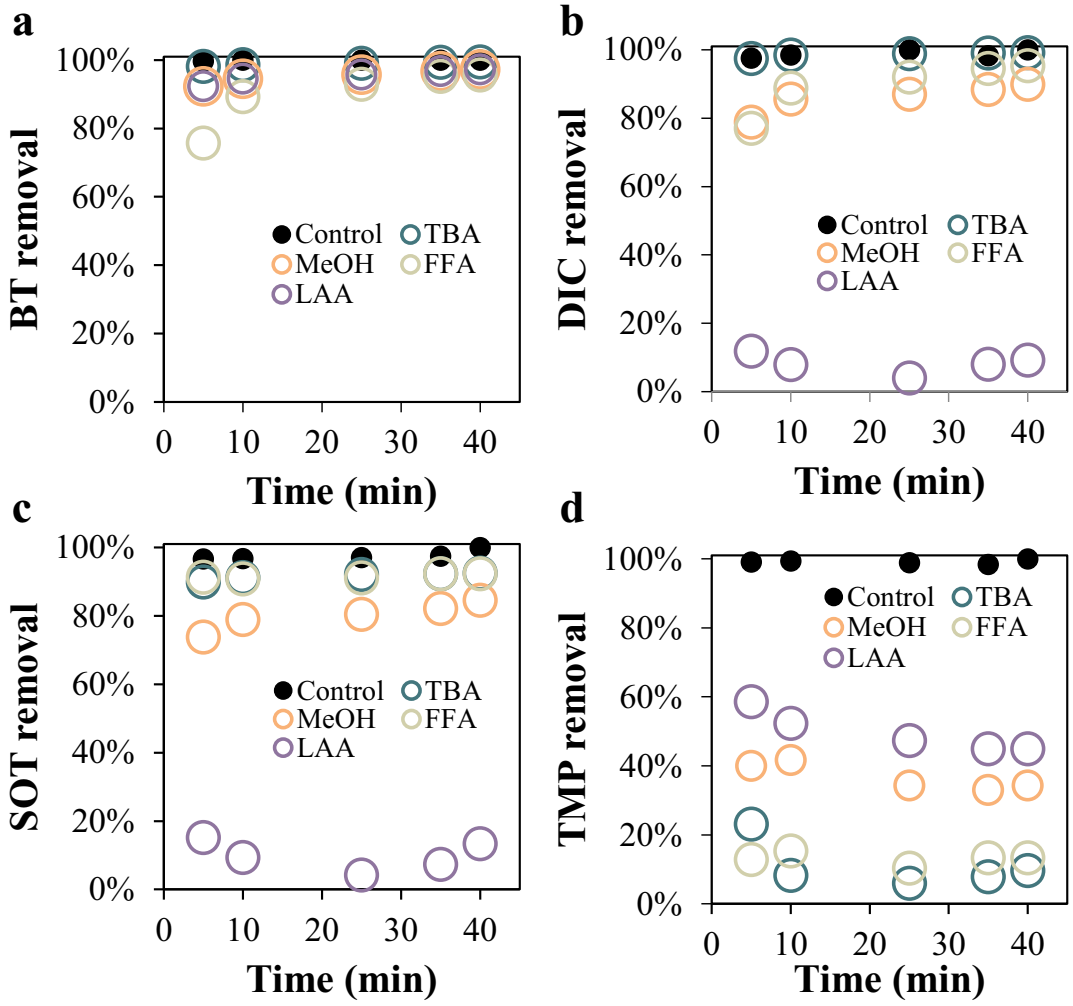

Fig. 7. Effects of different scavengers on OMP degradation during the filtration by the C30 membrane: (a) BT removal; (b) DIC removal; (c) SOT removal; and (d) TMP removal. TBA, MeOH, FFA, and LAA (0.4 mM) were individually added to a mixed solution containing 40 μM PMS and 5 μg/L of each OMP at pH 7. Filtration experiments were conducted using the C30 membrane at a constant flux of 30 L/(m^2 h).

qualitative approach, to comparatively evaluate the contribution of different RS to the degradation of individual OMPs in complex water matrices containing multiple OMPs.

Fig. 7a–d show the degradation efficacy of OMPs with the addition of different scavengers. It can be concluded that none of the scavengers had an inhibiting effect on the degradation of BT. However, the scavenger LAA considerably inhibited the degradation of DIC and SOT, reducing their degradation efficacies from 100% to 9%–13%. In addition, all scavengers contributed to the reduction of TMP degradation. Apparently, the degradation of BT was subjected to other RS pathways than foreseen, while DIC and SOT degradation were probably governed by $O_2^{\bullet-}$ oxidation. All the considered RS had an impact on TMP degradation. These results indicate that varying RS can be induced in PMS activated by alumina-supported Pd, and the degradation of multiple OMPs is largely dependent on the combined effects of different RS rather than any single specific species.

However, it should be noted that OMPs and the quenchers of FAA and LAA can also react rapidly with $^{\bullet}OH$ or $SO_4^{\bullet-}$ (Table S3). This indicates that the relatively low reaction kinetics between MeOH or TBA and $^{\bullet}OH$ or $SO_4^{\bullet-}$ likely limit their capacity in scavenging such radicals. Probably, surface-bound $SO_4^{\bullet-}$ radicals in PMS with alumina-supported Pd systems, as proposed by Feng et al. [9], can lead to a failure of quenching. The resistance of $^{\bullet}OH$ radicals, accumulated surrounding the heterogeneous catalysts to the TBA scavenger, has also been found by Zhang et al. [60]. The surface-bound radicals can be ascribed to the short diffusion distance of the radicals, which, consequently, led to a gradient of radical concentration in the membrane pores [51]. The above discussion thus suggests that $^{\bullet}OH$ and $SO_4^{\bullet-}$ probably play important roles in the degradation of the four OMPs.

The distinct degradation behaviors observed among the four target OMPs can also be elucidated by their structure-activity relationships governed by specific functional groups (Table 1). The fused triazole ring in BT exerts a strong electron-withdrawing effect, significantly reducing the electron density of its adjacent benzene ring. This structural stability makes BT recalcitrant to conventional RS attacks (Fig. 7a). DIC features an electron-donating secondary amine bridge connecting two aromatic rings, while SOT contains a sulfonamide group and protonated secondary amine (Table 1). $O_2^{\bullet-}$ was reported to preferentially attack the amine structures contained in DIC and SOT. As reported by Xiong et al., $O_2^{\bullet-}$ exhibits high selectivity toward amine architectures, promoting C—N bond activation and cleavage through single-electron transfer or hydrogen abstraction [61]. Hayyan et al. also demonstrated that $O_2^{\bullet-}$ acts as a strong nucleophile and Brønsted base, readily interacting with cationic amine groups via proton abstraction, or nucleophilic attack [62]. This also aligns with previous findings that $O_2^{\bullet-}$plays a critical role in the oxidative degradation of amine-containing pollutants such as diclofenac [63]. These nitrogen-containing functional groups therefore make DIC and SOT particularly susceptible to $O_2^{\bullet-}$ attack, rather than only attacked by the electrophilic RS such as $^{\bullet}OH$ and $SO_4^{\bullet-}$. TMP contains multiple electron-donating methoxy groups and amino groups, as well as a heteroaromatic pyrimidine ring. This TMP structure may provide multiple oxidation sites, explaining the collaborative inhibition observed with all scavengers (Fig. 7d) and its reported reactivity toward several RS, including $^{\bullet}OH$, $SO_4^{\bullet-}$, $O_2^{\bullet-}$, and $^1O_2$ (Table S3). Overall, these results indicate that the degradation of OMPs by RS can also be influenced by structure-activity relationships. Molecular features such as electron density and functional groups can influence the reactivity of OMPs toward different oxidative pathways. Further investigation is suggested to gain a deeper understanding of these relationships in future studies.

It should also be noted that we found that the identification of RS in Pd-UF-PMS systems is inherently dependent on the type of OMPs. As demonstrated by the quenching experiments using multiple representative OMPs, different scavenger effects were observed for BT, DIC, SOT, and TMP, indicating that multiple RS pathways contribute to the degradation. This means that the contribution of individual RS to OMPs depends on the target compound. Therefore, conclusions regarding a single dominant RS derived from single-OMP systems should be interpreted with caution, as such approaches may overlook the contributions of other RS pathways. Quantitative separation of individual RS contributions was beyond the scope of this study and requires further investigation.

Furthermore, the interpretation of scavenger experiments in PMS-based heterogeneous systems is intrinsically complex and should be paid attention. Recent studies have highlighted that commonly used scavengers are not fully selective and may participate in competing reactions with PMS or other RS, thereby affecting RS generation pathways rather than solely quenching them [30,64]. In addition, the effectiveness of scavengers is further constrained by the extremely short lifetimes of RS and their localized generation within membrane pores or at catalyst surfaces, where target OMPs may be enriched and react before scavengers can effectively compete [9,51]. Moreover, scavengers themselves may participate in side reactions with PMS or be transformed into reactive intermediates, thereby altering RS generation pathways rather than purely quenching them [30,65]. Taken together, the lack of significant inhibition by individual scavengers does not mean that the corresponding RS play a negligible role. Instead, it reflects the combined effects of RS interconversion, non-radical pathways, kinetic competition, and spatial confinement.

To further examine the potential involvement of Pd species during PMS activation, XPS spectra of the Pd-modified membrane were collected before and after the reaction with PMS (Figs. 2d and S15). After the long-term PMS exposure, the Pd^0 $3d_{5/2}$ peak shifted slightly from 335.3 to 335.5 eV. In addition, the relative fraction of Pd^0 decreased from 83.8% to 75.0%, whereas the fraction of Pd^{2+} increased from 16.2% to 25.0%. These changes suggest partial oxidation of Pd^0 and possible electron transfer from Pd sites to PMS during catalytic activation, implying the involvement of Pd^0/Pd^{2+} redox process. Similar Pd^0/Pd^{2+} transformations have been reported for Pd/ Al_2O_3 catalysts during catalytic oxidation reactions and were considered important for catalyst activity [66,67]. Furthermore, operando XPS studies have directly observed dynamic Pd^0/Pd^{2+} transformations during catalytic oxidation processes [66,67]. Pd^0/Pd^{2+} transitions have also been reported during oxidant activation processes (e.g., H_2O_2 and PMS), contributing to the generation of RS [17,68,69]. Nevertheless, a comprehensive understanding of the Pd-mediated PMS activation mechanism is beyond the scope of the present study and requires further operando characterization.

3.7. Degradation of OMPs from brine and river water

The degradation of OMPs from brine with a low (brine A) and high (brine B) salinity and from river water was performed to evaluate the potential application of the catalytic Pd-UF. The water quality parameters of these water types are shown in Table S1, where the main anions in the brine A, brine B, and the river water were Cl^- (16.4, 81.8, and 1.4 mM for brine A, brine B and river water, respectively), and SO_4^{2-} (18.4, 91.9, and 0.7 mM for brine A, brine B and river water, respectively), with a TDS of 4573, 22867, and 538 mg/L, respectively. The OMPs' degradation and PMS consumption in brine and river water are shown in Figs. 8 and S7.

In brine A (low salinity), the degradation of DIC and SOT was retained at a high efficacy of around 97%, while the degradation of BT and TMP was reduced to 82% and 65%, respectively. In brine B (higher salinity), the degradation efficacies of BT, SOT, and TMP dropped to 78%, 57%, and 16%, respectively, whereas DIC maintained a high degradation efficacy of 97%. These observations show that background ion interference is concentration-dependent. Compared to the minor impacts at 1 mM (Fig. 4e), the primary anions in brine A (16–19 mM) caused a moderate decrease in degradation of OMPs, which became significant in brine B (81–92 mM, Fig. 8b). This suggests that the degradation efficiency is gradually reduced by competitive reactions at

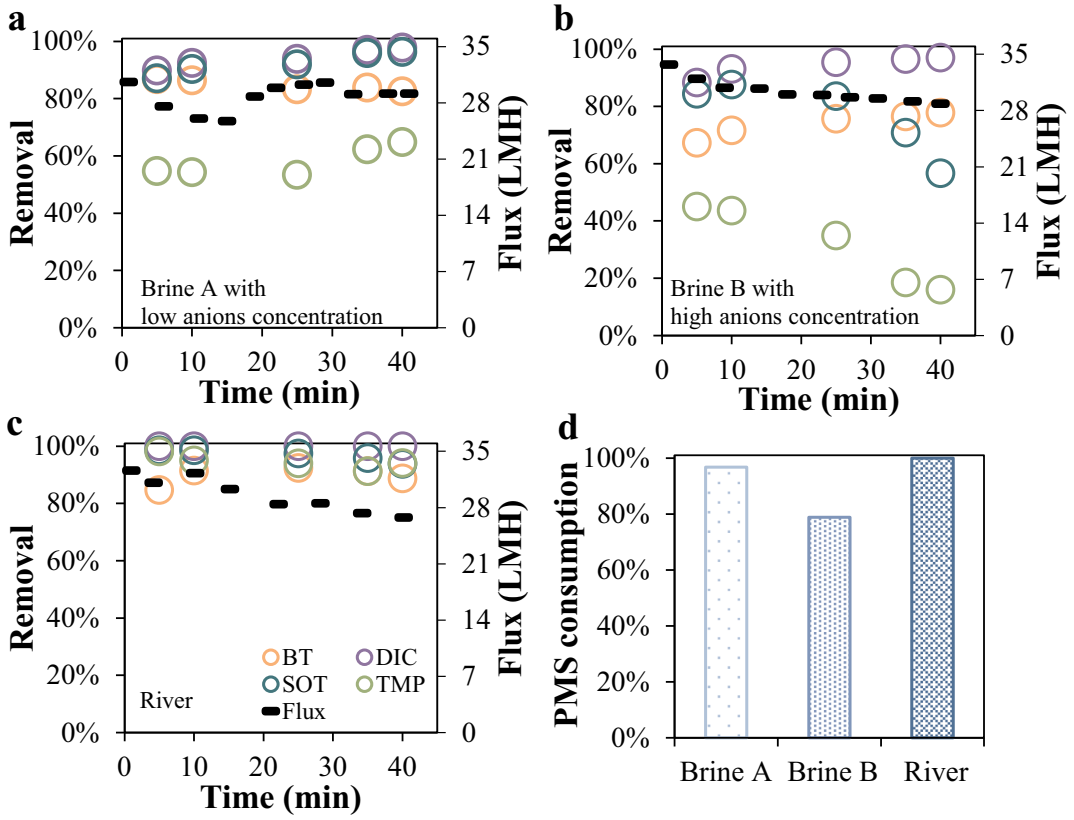

Fig. 8. OMP degradation performance in different water matrices: (a) degradation of OMPs in brine A with a low concentration of ions; (b) degradation of OMPs in brine B with a high concentration of ions; (c) degradation of OMPs in river water; and (d) PMS consumption in different water matrices after 40 min of filtration. Experiments were conducted using solutions containing 5 μg/L of each OMP and 40 μM PMS in brine A, brine B, and river water. Filtration was performed using the C30 membrane at a constant flux of 30 L/(m^2 h). PMS concentration was determined from the permeate samples collected during filtration.

higher anion concentrations. The negative impact of high ion concentrations on OMPs' degradation is consistent with the earlier study [50]. Fig. 8d shows that PMS consumption in brine B was reduced to 79%, compared to 97% in brine A, thereby inhibiting the degradation of OMPs. In addition to the reduced PMS availability caused by high salinity, other mechanisms such as RS scavenging, secondary RS generation, and competition for catalytic sites on the membrane surface have also been reported to induce inhibitory effects on OMPs' degradation. High brine anions (e.g., Cl^-) can scavenge primary strong RS and form low-activity secondary species (e.g., $Cl^•$ and $Cl_2^{•-}$) [34]. Anions can also compete with OMPs and PMS for catalytic sites on the membrane surface, further hindering contaminant adsorption and oxidation [70]. These mechanisms are likely to act synergistically, resulting in the observed inhibition of OMP degradation under high-salinity conditions [71]. However, the individual contributions of these mechanisms are beyond the scope of the present study and require further study.

High OMPs' degradation efficacies, ranging from 89%-100%, were kept during the duration of the experiment with river water, and all PMS was decomposed in this water type (Fig. 8c and d). These findings indicate that the main substance in the river water, i.e., the natural organic matters (NOM) (characterized by a total organic carbon concentration of 24 mg/L), had a minor impact on the degradation of OMPs and on the high PMS decomposition to induce RS.

4. Conclusion

This study demonstrates that ceramic UF membranes, conformally deposited with an ultra-low Pd loading via ALD, can effectively activate PMS for the degradation of OMPs. Compared to 3%–24% OMPs' removal via pristine UF membrane, the Pd-UF with PMS achieved near-complete removal of various OMPs, even at a high flux of 100 L/(m^2 h). This can be attributed to the nanoconfinement effect, which enriches OMPs and RS and improves their mass transfer in the confined-pore environment. Consistent with this, kinetic experiments showed that Pd deposited within the membrane pores increased degradation kinetics by three orders of magnitude compared to Pd located only on the membrane surface. Furthermore, quenching experiments showed that the dominant RS varied across different OMPs, highlighting the limitation of assigning the dominant RS based on the experiment by using a single OMP. For practical application, the system maintained high removal efficiency at neutral pH and in various water matrices, and was only marginally affected by common anions. Only extreme pH conditions or high salinity significantly suppressed degradation. Future research should focus on scaling up the deposition process, elucidating the contributions of different RS to the degradation of different OMPs, and optimizing performance under realistic operating conditions, thereby further advancing the practical applicability of this approach.

CRediT authorship contribution statement

Shuo Zhang: Writing – review & editing, Writing – original draft, Methodology, Investigation, Formal analysis, Data curation, Conceptualization. **Ming Li:** Writing – review & editing, Methodology, Investigation. **He Tian:** Methodology, Investigation. **J. Ruud van Ommen:** Writing – review & editing, Resources. **Luuk C. Rietveld:** Writing – review & editing, Supervision. **Sebastiaan G.J. Heijman:** Writing – review & editing, Supervision, Resources, Conceptualization.

Declaration of competing interest

The authors declare that they have no known competing financial interests or personal relationships that could have appeared to influence

the work reported in this paper.

Acknowledgements

The work was supported by China Scholarship Council (Grant number: 201808280006), and partially supported by Lamminga Foundation (the Netherlands). Dr. Mingliang Chen, and Dr. Bin Lin are acknowledged for their valuable and fruitful support and discussion, especially during the initiation of this project. We acknowledge WaterLab at TU Delft for the support in sample measurements. Our sincere thanks also go to Dr. Nadia van Pelt (TU Delft, The Netherlands) for her assistance with the language and grammar of the manuscript.

Appendix A. Supplementary data

Supplementary data to this article can be found online at https://doi.org/10.1016/j.seppur.2026.139029.

Data availability

Data will be made available on request.

References

[1] M. Fu, J. Wang, B. Heijman, J.P. van der Hoek, Removal of organic micropollutants by well-tailored granular zeolites and subsequent ozone-based regeneration, J. Water Process Eng. 44 (2021) 102403, https://doi.org/10.1016/j.jwpe.2021.102403.
[2] M. Chen, S.G.J. Heijman, M.W.J. Luiten-Olieman, L.C. Rietveld, Oil-in-water emulsion separation: fouling of alumina membranes with and without a silicon carbide deposition in constant flux filtration mode, Water Res. 216 (2022) 118267, https://doi.org/10.1016/j.watres.2022.118267.
[3] S. Zhang, Y. Liang, C. Yang, P. Venema, L.C. Rietveld, S.G.J. Heijman, Concentration polarizations of PEG and silica colloids in ceramic nanofiltration, Desalination 583 (2024) 117722, https://doi.org/10.1016/j.desal.2024.117722.
[4] J.L. Acero, F.J. Benitez, F.J. Real, E. Rodriguez, Elimination of selected emerging contaminants by the combination of membrane filtration and chemical oxidation processes, Water Air Soil Pollut. 226 (2015) 139, https://doi.org/10.1007/s11270-015-2404-8.
[5] W.-C. Huang, M. Liu, F.-G. Zhang, D. Li, Y. Du, Y. Chen, Q.-Y. Wu, Removal of disinfection byproducts and toxicity of chlorinated water by post-treatments of ultraviolet/hydrogen peroxide and ultraviolet /peroxymonosulfate, J. Clean. Prod. 352 (2022) 131563, https://doi.org/10.1016/j.jclepro.2022.131563.
[6] M. Ran, T. Gong, Z. Tang, M. Ran, T. Gong, Z. Tang, Removal of new contaminants from wastewater through advanced oxidation processes - a perspective, New Contam. 1 (2025), https://doi.org/10.48130/newcontam-0025-0020.
[7] T.E. Berger, C. Regmi, A.I. Schäfer, B.S. Richards, Photocatalytic degradation of organic dye via atomic layer deposited TiO2 on ceramic membranes in single-pass flow-through operation, J. Membr. Sci. 604 (2020) 118015, https://doi.org/10.1016/j.memsci.2020.118015.
[8] W. Ma, M. Sun, D. Huang, C. Chu, T. Hedtke, X. Wang, Y. Zhao, J.-H. Kim, M. Elimelech, Catalytic membrane with copper single-atom catalysts for effective hydrogen peroxide activation and pollutant destruction, Environ. Sci. Technol. 56 (2022) 8733–8745, https://doi.org/10.1021/acs.est.1c08937.
[9] Y. Feng, P.-H. Lee, D. Wu, K. Shih, Surface-bound sulfate radical-dominated degradation of 1,4-dioxane by alumina-supported palladium (Pd/Al2O3) catalyzed peroxymonosulfate, Water Res. 120 (2017) 12–21, https://doi.org/10.1016/j.watres.2017.04.070.
[10] X. Wu, K. Rigby, D. Huang, T. Hedtke, X. Wang, M.W. Chung, S. Weon, E. Stavitski, J.-H. Kim, Single-atom cobalt incorporated in a 2D graphene oxide membrane for catalytic pollutant degradation, Environ. Sci. Technol. 56 (2022) 1341–1351, https://doi.org/10.1021/acs.est.1c06371.
[11] Y. Cheng, Z. Chen, S. Wang, X. Duan, Single atom catalysts for heterogeneous catalytic ozonation, Curr. Opin. Chem. Eng. 41 (2023) 100945, https://doi.org/10.1016/j.coche.2023.100945.
[12] M. Li, S. Saedy, S. Fu, T. Stellema, R. Kortlever, J.R. van Ommen, Enhancing the durability of Pt nanoparticles for water electrolysis using ultrathin SiO2 layers, Catal. Sci. Technol. 14 (2024) 1328–1335, https://doi.org/10.1039/D3CY00996C.
[13] S. Lotfi, K. Fischer, A. Schulze, A.I. Schäfer, Photocatalytic degradation of steroid hormone micropollutants by TiO2-coated polyethersulfone membranes in a continuous flow-through process, Nat. Nanotechnol. 17 (2022) 417–423, https://doi.org/10.1038/s41565-022-01074-8.
[14] K.L. Pickrahn, A. Garg, S.F. Bent, ALD of ultrathin ternary oxide Electrocatalysts for water splitting, ACS Catal. 5 (2015) 1609–1616, https://doi.org/10.1021/cs501532b.
[15] J.S. King, A. Wittstock, J. Biener, S.O. Kucheyev, Y.M. Wang, T.F. Baumann, S. K. Giri, A.V. Hamza, M. Baeumer, S.F. Bent, Ultralow loading Pt Nanocatalysts prepared by atomic layer deposition on carbon aerogels, Nano Lett. 8 (2008) 2405–2409, https://doi.org/10.1021/nl801299z.
[16] Z. Song, M. Norouzi Banis, H. Liu, L. Zhang, Y. Zhao, J. Li, K. Doyle-Davis, R. Li, S. Knights, S. Ye, G.A. Botton, P. He, X. Sun, Ultralow loading and high-performing Pt catalyst for a polymer electrolyte membrane fuel cell anode achieved by atomic layer deposition, ACS Catal. 9 (2019) 5365–5374, https://doi.org/10.1021/acscatal.8b04504.
[17] Y.-Y. Ahn, H. Bae, H.-I. Kim, S.-H. Kim, J.-H. Kim, S.-G. Lee, J. Lee, Surface-loaded metal nanoparticles for peroxymonosulfate activation: efficiency and mechanism reconnaissance, Appl. Catal. B Environ. 241 (2019) 561–569, https://doi.org/10.1016/j.apcatb.2018.09.056.
[18] J.W. Elam, A. Zinovev, C.Y. Han, H.H. Wang, U. Welp, J.N. Hryn, M.J. Pellin, Atomic layer deposition of palladium films on Al2O3 surfaces, Thin Solid Films 515 (2006) 1664–1673, https://doi.org/10.1016/j.tsf.2006.05.049.
[19] L. Kong, G. Fang, X. Xi, Y. Wen, Y. Chen, M. Xie, F. Zhu, D. Zhou, J. Zhan, A novel peroxymonosulfate activation process by periclase for efficient singlet oxygen-mediated degradation of organic pollutants, Chem. Eng. J. 403 (2021) 126445, https://doi.org/10.1016/j.cej.2020.126445.
[20] Y.-Y. Ahn, E.-T. Yun, J.-W. Seo, C. Lee, S.H. Kim, J.-H. Kim, J. Lee, Activation of peroxymonosulfate by surface-loaded noble metal nanoparticles for oxidative degradation of organic compounds, Environ. Sci. Technol. 50 (2016) 10187–10197, https://doi.org/10.1021/acs.est.6b02841.
[21] H.V. Bui, F. Grillo, J.R. van Ommen, Atomic and molecular layer deposition: off the beaten track, Chem. Commun. 53 (2016) 45–71, https://doi.org/10.1039/C6CC05568K.
[22] K.S. Yoo, D.-G. Kim, S. Lee, W.-B. Lee, J.-S. Park, Atmospheric pressure spatial ALD of Al2O3 thin films for flexible PEALD IGZO TFT application, Ceram. Int. 48 (2022) 18803–18810, https://doi.org/10.1016/j.ceramint.2022.03.157.
[23] D.H. Levy, D. Freeman, S.F. Nelson, P.J. Cowdery-Corvan, L.M. Irving, Stable ZnO thin film transistors by fast open air atomic layer deposition, Appl. Phys. Lett. 92 (2008) 192101, https://doi.org/10.1063/1.2924768.
[24] D. Fang, F. He, J. Xie, L. Xue, Calibration of binding energy positions with C1s for XPS results, J. Wuhan Univ. Technol.-Mater Sci Ed 35 (2020) 711–718, https://doi.org/10.1007/s11595-020-2312-7.
[25] M. Chen, L. Zhu, J. Chen, F. Yang, C.Y. Tang, M.D. Guiver, Y. Dong, Spinel-based ceramic membranes coupling solid sludge recycling with oily wastewater treatment, Water Res. 169 (2020) 115180, https://doi.org/10.1016/j.watres.2019.115180.
[26] L. Lin, C. Feng, R. Lopez, O. Coronell, Identifying facile and accurate methods to measure the thickness of the active layers of thin-film composite membranes – a comparison of seven characterization techniques, J. Membr. Sci. 498 (2016) 167–179, https://doi.org/10.1016/j.memsci.2015.09.059.
[27] M. Fu, B. Heijman, J.P. van der Hoek, Removal of organic micropollutants from wastewater effluent: selective adsorption by a fixed-bed granular zeolite filter followed by in-situ ozone-based regeneration, Sep. Purif. Technol. 303 (2022) 122303, https://doi.org/10.1016/j.seppur.2022.122303.
[28] M. Azzi, S. Ravier, A. Elkak, B. Coulomb, J.-L. Boudenne, Fast UHPLC-MS/MS for the simultaneous determination of azithromycin, erythromycin, fluoxetine and Sotalol in surface water samples, Appl. Sci. 11 (2021) 8316, https://doi.org/10.3390/app11188316.
[29] PubChem, PubChem, (n.d.). https://pubchem.ncbi.nlm.nih.gov/ (accessed April 8, 2025).
[30] L. Gao, Y. Guo, J. Zhan, G. Yu, Y. Wang, Assessment of the validity of the quenching method for evaluating the role of reactive species in pollutant abatement during the persulfate-based process, Water Res. 221 (2022) 118730, https://doi.org/10.1016/j.watres.2022.118730.
[31] A. Nandi, I.B. Chatterjee, Scavenging of superoxide radical by ascorbic acid, J. Biosci. 11 (1987) 435–441, https://doi.org/10.1007/BF02704692.
[32] M.E.A. Ali, Nanofiltration process for enhanced treatment of RO brine discharge, Membranes 11 (2021) 212, https://doi.org/10.3390/membranes11030212.
[33] C.R. Martinetti, A.E. Childress, T.Y. Cath, High recovery of concentrated RO brines using forward osmosis and membrane distillation, J. Membr. Sci. 331 (2009) 31–39, https://doi.org/10.1016/j.memsci.2009.01.003.
[34] Y. Yang, J.J. Pignatello, J. Ma, W.A. Mitch, Effect of matrix components on UV/H2O2 and UV/S2O82− advanced oxidation processes for trace organic degradation in reverse osmosis brines from municipal wastewater reuse facilities, Water Res. 89 (2016) 192–200, https://doi.org/10.1016/j.watres.2015.11.049.
[35] C. Liang, C.-F. Huang, N. Mohanty, R.M. Kurakalva, A rapid spectrophotometric determination of persulfate anion in ISCO, Chemosphere 73 (2008) 1540–1543, https://doi.org/10.1016/j.chemosphere.2008.08.043.
[36] J. Lu, P.C. Stair, Nano/subnanometer Pd nanoparticles on oxide supports synthesized by AB-type and low-temperature ABC-type atomic layer deposition: growth and morphology, Langmuir 26 (2010) 16486–16495, https://doi.org/10.1021/la101378s.
[37] M.J. Weber, A.J.M. Mackus, M.A. Verheijen, V. Longo, A.A. Bol, W.M.M. Kessels, Atomic layer deposition of high-purity palladium films from Pd(hfac)2 and H2 and O2 plasmas, J. Phys. Chem. C 118 (2014) 8702–8711, https://doi.org/10.1021/jp5009412.
[38] A. Datta, S. Deolka, P. Kumar, Z. Ziadi, T. Sasaki, S. Steinhauer, V. Singh, N. Jian, E. Danielson, A.J. Porkovich, In situ investigation of oxidation across a heterogeneous nanoparticle–support interface during metal support interactions, Phys. Chem. Chem. Phys. 23 (2021) 2063–2071, https://doi.org/10.1039/D0CP05697A.
[39] M. Li, S. Fu, S. Saedy, A. Rajendrakumar, F.D. Tichelaar, R. Kortlever, J.R. van Ommen, Nanostructuring Pt-Pd bimetallic electrocatalysts for CO2 reduction using atmospheric pressure atomic layer deposition, ChemCatChem 14 (2022) e202200949, https://doi.org/10.1002/cctc.202200949.

[40] M.C. Militello, S.J. Simko, Elemental palladium by XPS, Surf. Sci. Spectra 3 (1994) 387–394, https://doi.org/10.1116/1.1247783.
[41] M.C. Militello, S.J. Simko, Palladium oxide (PdO) by XPS, Surf. Sci. Spectra 3 (1994) 395–401, https://doi.org/10.1116/1.1247784.
[42] R. Salehi, S.M. Mousavi, M. Taherian, Assessment of micellar-enhanced ultrafiltration process performance for removal of pharmaceutical contaminant from wastewater using response surface methodology, Int. J. Environ. Sci. Technol. 16 (2019) 6199–6206, https://doi.org/10.1007/s13762-018-2021-3.
[43] F. Ghanbari, M. Moradi, Application of peroxymonosulfate and its activation methods for degradation of environmental organic pollutants: review, Chem. Eng. J. 310 (2017) 41–62, https://doi.org/10.1016/j.cej.2016.10.064.
[44] I. Levitsky, D. Tavor, V. Gitis, Microbubbles and organic fouling in flat sheet ultrafiltration membranes, Sep. Purif. Technol. 268 (2021) 118710, https://doi.org/10.1016/j.seppur.2021.118710.
[45] S. Liu, P.C. Edara, A.I. Schäfer, Influence of organic matter on the photocatalytic degradation of steroid hormones by TiO2-coated polyethersulfone microfiltration membrane, Water Res. 245 (2023) 120438, https://doi.org/10.1016/j.watres.2023.120438.
[46] H. Kang, D. Lee, K.-M. Lee, H.-H. Kim, H. Lee, M. Sik Kim, C. Lee, Nonradical activation of peroxymonosulfate by hematite for oxidation of organic compounds: a novel mechanism involving high-valent iron species, Chem. Eng. J. 426 (2021) 130743, https://doi.org/10.1016/j.cej.2021.130743.
[47] C. Dong, Z. Wang, Z. Ye, J. He, Z. Zheng, X. Gong, J. Zhang, I.M.C. Lo, Superoxide radicals dominated visible light driven peroxymonosulfate activation using molybdenum selenide (MoSe2) for boosting catalytic degradation of pharmaceuticals and personal care products, Appl. Catal. B Environ. 296 (2021) 120223, https://doi.org/10.1016/j.apcatb.2021.120223.
[48] S.-W. Nam, D.-J. Choi, S.-K. Kim, N. Her, K.-D. Zoh, Adsorption characteristics of selected hydrophilic and hydrophobic micropollutants in water using activated carbon, J. Hazard. Mater. 270 (2014) 144–152, https://doi.org/10.1016/j.jhazmat.2014.01.037.
[49] S.-W. Nam, B.-I. Jo, Y. Yoon, K.-D. Zoh, Occurrence and removal of selected micropollutants in a water treatment plant, Chemosphere 95 (2014) 156–165, https://doi.org/10.1016/j.chemosphere.2013.08.055.
[50] Y. Wang, S. Hui, S. Zhan, R. Djellabi, J. Li, X. Zhao, Activation of peroxymonosulfate by novel Pt/Al2O3 membranes via a nonradical mechanism for efficient degradation of electron-rich aromatic pollutants, Chem. Eng. J. 381 (2020) 122563, https://doi.org/10.1016/j.cej.2019.122563.
[51] S. Zhang, M. Sun, T. Hedtke, A. Deshmukh, X. Zhou, S. Weon, M. Elimelech, J.-H. Kim, Mechanism of heterogeneous Fenton reaction kinetics enhancement under nanoscale spatial confinement, Environ. Sci. Technol. 54 (2020) 10868–10875, https://doi.org/10.1021/acs.est.0c02192.
[52] C. Meng, B. Ding, S. Zhang, L. Cui, K.K. Ostrikov, Z. Huang, B. Yang, J.-H. Kim, Z. Zhang, Angstrom-confined catalytic water purification within co-TiOx laminar membrane nanochannels, Nat. Commun. 13 (2022) 4010, https://doi.org/10.1038/s41467-022-31807-1.
[53] J. Chang, B. Yu, X. Peng, P. Zhang, X. Xu, Nanoconfined catalytic macrostructures for advanced water remediation: from basic understanding to future application strategies, Water Res. 272 (2025) 122960, https://doi.org/10.1016/j.watres.2024.122960.
[54] S. Zhang, T. Hedtke, Q. Zhu, M. Sun, S. Weon, Y. Zhao, E. Stavitski, M. Elimelech, J.-H. Kim, Membrane-confined iron oxychloride nanocatalysts for highly efficient heterogeneous Fenton water treatment, Environ. Sci. Technol. 55 (2021) 9266–9275, https://doi.org/10.1021/acs.est.1c01391.
[55] S. Liu, A.I. Schäfer, Identification and quantification of reactive oxygen species in photocatalytic membrane reactors: reassessment of the validity of methods, Chem. Rev. (2026), https://doi.org/10.1021/acs.chemrev.5c01120 acs.chemrev.5c01120.
[56] W. Li, G. Song, J. Jing, X. Ren, C. Zhang, M.A. Oturan, M. Zhou, Identification and quantification of reactive species in aqueous medium during application of advanced oxidation processes: a critical review, Chem. Eng. J. 500 (2024) 156698, https://doi.org/10.1016/j.cej.2024.156698.
[57] J. Yan, H. Liu, C. Dou, Y. Wu, W. Dong, Quantitative probing of reactive oxygen species and their selective degradation on contaminants in peroxymonosulfate-based process enhanced by picolinic acid, J. Hazard. Mater. 459 (2023) 132083, https://doi.org/10.1016/j.jhazmat.2023.132083.
[58] H. Liu, J. Zhao, Y. Wang, Y. Wu, W. Dong, M. Nie, X. Wang, Enhancement of peroxymonosulfate activation by sinapic acid accelerating Fe(III)/Fe(II) cycle, Chem. Eng. J. 446 (2022) 137177, https://doi.org/10.1016/j.cej.2022.137177.
[59] K. Zhou, Z. Wang, X. Wang, G. Jiao, Y. Li, S.-P. Sun, X.D. Chen, Degradation of emerging pharmaceutical micropollutants in municipal secondary effluents by low-pressure UVC-activated HSO5− and S2O82− AOPs, Chem. Eng. J. 393 (2020) 124712, https://doi.org/10.1016/j.cej.2020.124712.
[60] S. Zhang, X. Quan, J.-F. Zheng, D. Wang, Probing the interphase "HO zone" originated by carbon nanotube during catalytic ozonation, Water Res. 122 (2017) 86–95, https://doi.org/10.1016/j.watres.2017.05.063.
[61] K. Xiong, F. Zhang, Y. Wang, B. Zeng, X. Lang, Selective oxidation of amines powered with green light and oxygen over an anthraquinone covalent organic framework, J. Colloid Interface Sci. 643 (2023) 340–349, https://doi.org/10.1016/j.jcis.2023.04.017.
[62] M. Hayyan, M.A. Hashim, I.M. AlNashef, Superoxide ion: generation and chemical implications, Chem. Rev. 116 (2016) 3029–3085, https://doi.org/10.1021/acs.chemrev.5b00407.
[63] Q. Zhang, C. Tan, X. Zheng, P. Chen, M. Zhuo, T. Chen, Z. Xie, F. Wang, H. Liu, Y. Liu, X. Zhang, W. Lv, G. Liu, Dual metal-free polymer reactive sites for the efficient degradation of diclofenac by visible light-driven oxygen reduction to superoxide radical and hydrogen peroxide, Environ. Sci. Nano 6 (2019) 2577–2590, https://doi.org/10.1039/C9EN00482C.
[64] B. Huang, Z. Wu, J. Zhang, Y. Shi, C.-S. He, Z. Xiong, B. Lai, Is the choice of quencher appropriate for exploring reactive oxygen species in advanced oxidation processes? Chin. Chem. Lett. 37 (2026) 111537 https://doi.org/10.1016/j.cclet.2025.111537.
[65] R. Xiao, Z. Luo, Z. Wei, D. Minakata, R. Spinney, S. Wacławek, W. Zeng, C. Tang, Beyond the bench: evaluating the reliability of chemical scavengers in radical-based advanced oxidation processes, 2024, https://doi.org/10.2139/ssrn.5011850.
[66] K. Zorn, S. Giorgio, E. Halwax, C.R. Henry, H. Grönbeck, G. Rupprechter, CO oxidation on technological Pd−Al2O3 catalysts: oxidation state and activity, J. Phys. Chem. C 115 (2011) 1103–1111, https://doi.org/10.1021/jp106235x.
[67] G.B. Hoflund, H.A.E. Hagelin, J.F. Weaver, G.N. Salaita, ELS and XPS study of Pd/PdO methane oxidation catalysts, Appl. Surf. Sci. 205 (2003) 102–112, https://doi.org/10.1016/S0169-4332(02)01084-X.
[68] V.R. Choudhary, C. Samanta, P. Jana, Decomposition and/or hydrogenation of hydrogen peroxide over Pd/Al2O3 catalyst in aqueous medium: factors affecting the rate of H2O2 destruction in presence of hydrogen, Appl. Catal. A Gen. 332 (2007) 70–78, https://doi.org/10.1016/j.apcata.2007.08.004.
[69] Y. Wang, D. Cao, M. Liu, X. Zhao, Insights into heterogeneous catalytic activation of peroxymonosulfate by Pd/g-C3N4: the role of superoxide radical and singlet oxygen, Catal. Commun. 102 (2017) 85–88, https://doi.org/10.1016/j.catcom.2017.08.016.
[70] A. Piscopo, D. Robert, J.V. Weber, Influence of pH and chloride anion on the photocatalytic degradation of organic compounds: part I. Effect on the benzamide and Para-hydroxybenzoic acid in TiO2 aqueous solution, Appl. Catal. B Environ. 35 (2001) 117–124, https://doi.org/10.1016/S0926-3373(01)00244-2.
[71] S.P. Azerrad, S. Gur-Reznik, L. Heller-Grossman, C.G. Dosoretz, Advanced oxidation of iodinated X-ray contrast media in reverse osmosis brines: the influence of quenching, Water Res. 62 (2014) 107–116, https://doi.org/10.1016/j.watres.2014.05.041.